Dalton Transactions

ROYAL SOCIETY OF CHEMISTRY

PAPER

View Article Online
View Journal | View Issue

Cite this: *Dalton Trans.*, 2026, **55**, 663

Hydroboration of carbonyl compounds catalysed by a molybdenum germylyne complex: metal–ligand cooperative mechanism

Christof Fontanilla,[a] Yuto Shimizu,[b] Koichi Nagata,[a] Sakura Iwatsuki,[a] Aoi Tanamura,[a] Seiji Mori,*[b] Tara Prasad Dhungana[a] and Hisako Hashimoto*[a]

Received 26th November 2025,
Accepted 12th December 2025

DOI: 10.1039/d5dt02829a

rsc.li/dalton

A molybdenum germylyne complex with a Mo≡Ge triple bond promotes the catalytic hydroboration of aldehydes and ketones with HBpin. Hydroboration of aldehydes proceeded efficiently at ambient temperature, affording the corresponding borate esters in 92–99% NMR yields, whereas hydroboration of ketones required a slight elevated temperature (70 °C), affording the products in 90–96% NMR yields. Mechanistic investigations, including KIE experiments, kinetic analyses and DFT calculations suggest a unique metal–ligand cooperative mechanism at the Mo≡Ge bond that promotes hydroboration of substrates through a six-membered-ring transition state during the rate-determining step.

Introduction

Catalytic hydroboration of unsaturated compounds using boranes has emerged as a powerful synthetic strategy, enabling reductions without the need for stoichiometric metal hydride reagents such as $NaBH_4$ or $LiAlH_4$.[1–6] The resulting organoboron products serve as versatile intermediates for a broad range of synthetic transformations. In particular, the catalytic hydroboration of carbonyl compounds has been established as an efficient route to functionalized alcohols, thereby stimulating the development of diverse molecular catalysts. Transition-metal-based systems represent a major class and continue to expand in scope, while increasing attention has recently been directed toward main-group catalysts, including those derived from s-block and p-block elements.[1,4,7] Within this expanding landscape of catalyst design, mechanistic studies have also advanced, with notable contributions from frustrated Lewis pairs,[8] bifunctional architectures and metal–ligand cooperative systems.[9,10]

From the bifunctional and cooperative perspectives,[11] low-valent main-group species, such as tetrylenes and tetrylene transition-metal complexes featuring divalent heavier group 14 elements, have attracted considerable attention as a new class of molecular activation platforms.[7,11–13] Recent intensive studies have revealed their remarkable ability to activate small molecules, including σ-bonds and unsaturated bonds, which is ascribed to their low-coordinate and unique electronic structures (bearing both Lewis base and Lewis acid moieties), ultimately leading to the discovery of their catalytic performance. Tetrylene species[7,13–17] such as germylene **A**,[9a] stannylene **B**[16a] and silylene **C**,[17a] illustrated in Fig. 1, have been reported to act as precatalysts or catalysts for the hydroboration of alde-

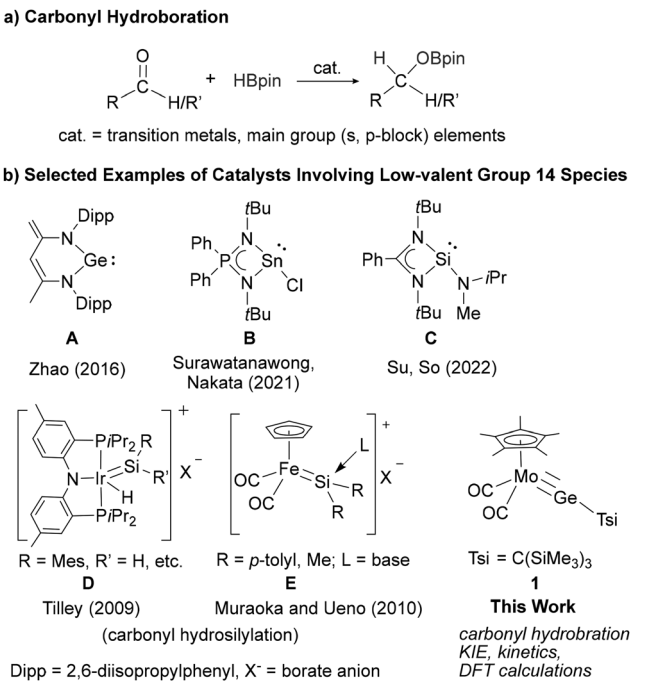

Fig. 1 (a) Carbonyl hydroboration and (b) selected examples of catalysts involving low-valent group 14 species.

[a]*Department of Chemistry, Graduate School of Science, Tohoku University, 6-3 Aoba, Sendai, Miyagi, 980-8578, Japan. E-mail: hisako.hashimoto.b7@tohoku.ac.jp*
[b]*Institute of Quantum Beam Science, Graduate School of Science and Engineering, Ibaraki University, 2-1-1 Bunkyo, Mito, Ibaraki, 310-8512, Japan*

hydes and ketones. Although detailed mechanistic studies remain limited, tetrylene hydride species are widely regarded as key intermediates initiating carbonyl activation at the tetrel centre, whereas the germylene **A** system is proposed to operate *via* metal–ligand cooperation.

In the case of tetrylene complexes, catalytic performance has also been demonstrated. For example, several silylene complexes featuring M=Si bonds have been shown to catalyse the hydrosilylation of carbonyl compounds, as reported by Tilley *et al.* using iridium silylene complex **D**,[18c] and by Muraoka and Ueno's group using iron silylene complex **E**.[19] In these cases, the electrophilic tetrel centre is also regarded to act as the initial activator of the carbonyls rather than the metal centre, with subsequent catalysis achieved through the cooperative action of both the metal and the tetrel centres, namely, metal–ligand cooperation is operative. In these systems, however, catalytic hydroboration reactions have not yet been reported.

Furthermore, monovalent tetrylyne complexes remain far less explored despite their distinct electronic structures and promising reactivity,[20] and thus represent an emerging frontier in catalyst design. Recently, our group discovered that the germylyne complex $Cp^*(OC)_2Mo{\equiv}GeC(SiMe_3)_3$ (**1**),[21] featuring a monovalent germanium ligand, can catalyse the hydrosilylation of aldehydes and ketones.[22,23] We further found that the same complex can catalyse hydroboration. Herein, we present experimental results of hydroboration reactions catalysed by the molybdenum germylyne complex **1**, alongside mechanistic investigations combining kinetic experiments and DFT calculations. These studies elucidate the cooperative roles of the Mo and Ge centres in substrate activation and transformation, providing a comprehensive understanding of the reaction pathway in this new system.

Results and discussion

Catalytic hydroboration of aldehydes and ketones by complex 1

The catalytic activity of the molybdenum germylyne complex **1** was first examined in the hydroboration of benzaldehyde **2a** with HBpin (pin = pinacolate). Prior to this, we benchmarked the transformation of **2a** with HBpin under otherwise identical conditions, both in the absence and presence of complex **1**, since aldehydes are known to undergo hydroboration with HBpin under neat conditions even in the absence of a catalyst.[24] In the absence of the catalyst, the reaction proceeded only slightly (Fig. S1 in SI), consistent with the reported uncatalysed reactivity.[24] When **2a** (1.0 eq.) and HBpin (1.5 eq.) were treated with 10 mol% of complex **1** in toluene under an inert atmosphere at 25 °C, the corresponding hydroboration product $PhCH_2OBpin$ (**3a**) was obtained in 98% NMR yield (Table 1, entry 1). These results indicate that complex **1** serves as an effective catalyst for the hydroboration, significantly enhancing the reaction efficiency.

To further explore the scope of this catalytic system, we next examined the hydroboration of various aldehydes under similar conditions (0.10 M solutions, 10 mol% **1**, 1.5 eq. HBpin). The hydroboration products **3a–3i** were identified by comparing their NMR data with previously reported ^{1}H, ^{13}C{^{1}H} and ^{11}B{^{1}H} NMR spectra (see SI for details). As summarised in Table 1, the reaction proceeded at room temperature (25 °C) smoothly across a broad range of substrates, affording the corresponding hydroboration products in high yields. Both aryl-substituted (entries 1–5) and alkyl-substituted (entries 6–8) aldehydes were well tolerated, highlighting the generality of **1** as a catalyst. Notably, the catalyst was also competent in effecting double hydroboration of dialdehyde substrates (entry 9), further demonstrating its synthetic versatility. In the comparison of *para*-substituted arylaldehydes, all derivatives tested afforded the corresponding products in high yields (entries 1–5), regardless of whether electron-withdrawing or

Table 1 Substrate scope for hydroboration of aldehydes (**2a–2i**) catalysed by **1**

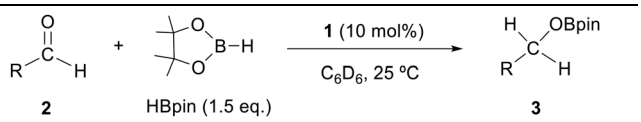

2 **3**

Entry	Aldehyde	Product	NMR yield/%	*t*/h
1	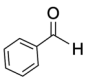 **2a**	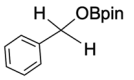 **3a**	98	20
2	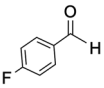 **2b**	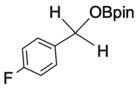 **3b**	93	25
3	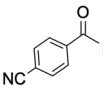 **2c**	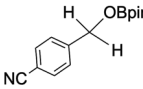 **3c**	98	25
4	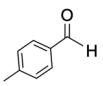 **2d**	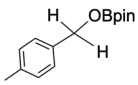 **3d**	98	24
5	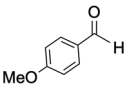 **2e**	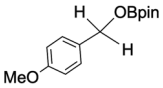 **3e**	99	23
6	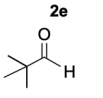 **2f**	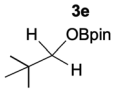 **3f**	92	25
7	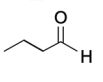 **2g**	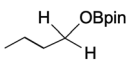 **3g**	92	4
8	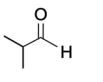 **2h**	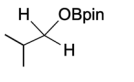 **3h**	97	5
9[a]	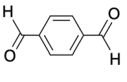 **2i**	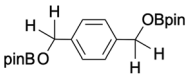 **3i**	99	21

[a] 3 eq. of HBpin was used.

electron-donating groups were introduced. These results indicate that the effect of *para*-substituents is relatively minor under the present reaction conditions (*vide infra*). On the other hand, steric effects were observed for alkyl-substituted aldehydes. Aldehydes bearing linear or moderately branched alkyl groups (entries 7 and 8) reacted at significantly faster rates, whereas the presence of a bulky *tert*-butyl group (entry 6) led to a marked decrease in reactivity.

Having confirmed that complex **1** effectively catalyses the hydroboration of aldehydes, we next investigated its activity toward ketones (Table 2), using the same conditions as in Table 1 but at an elevated temperature of 70 °C. These ketones include monoaryl, diaryl, polycyclic, linear, monocyclic, and branched aliphatic groups; acetophenone **4a**, benzophenone **4b**, 2-adamantanone **4c**, 2-butanone **4d**, acetylcyclohexane **4e** and pinacolone **4f**. Hydroboration of these ketones afforded the corresponding products in 90–96% yields. Steric effects, as observed for aldehydes, strongly affect the reaction rate, as indicated by the comparisons between entries 1 and 2 and entries 5 and 6; bulkier substrates require much longer reaction times. This is likely due to steric hindrance from the bulky Tsi substituent on the germanium centre.

Compared to other catalytic hydroboration systems, complex **1** can still be regarded as a catalyst in its early stage of development. The TOFs (h^{-1}) for aldehydes listed in Table 1 range from 0.4 to 2.0, whereas those for ketones in Table 2 range from 0.02 to 0.20. For example, in the hydroboration of benzaldehyde, the TOF for complex **1** is 0.5 h^{-1}, which is much lower than that of stannylene **B** (198 h^{-1}),[16a] but comparable to or slightly below that of germylene **A** (2.1 h^{-1})[9a,25] and silylene **C** (3.3 h^{-1}).[17a] Although its current performance is limited, complex **1** effectively promotes hydroboration across a broad range of carbonyl substrates, providing a basis for a new catalytic platform for this transformation.

Table 2 Substrate scope for hydroboration of ketones (**4a–4f**) catalysed by **1**

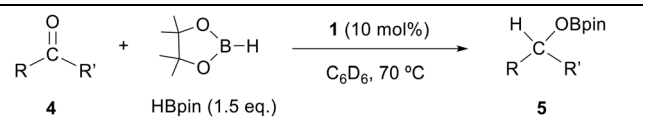

4 HBpin (1.5 eq.) **5**

Entry	Ketone	Product	NMR yield/%	*t*/h
1	 **4a**	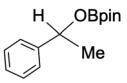 **5a**	96	144
2	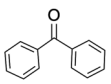 **4b**	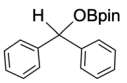 **5b**	90	211
3	 **4c**	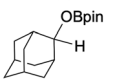 **5c**	93	55
4	 **4d**	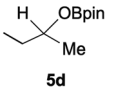 **5d**	94	49
5	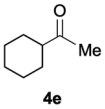 **4e**	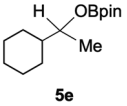 **5e**	93	130
6	 **4f**	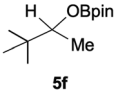 **5f**	91	563

KIE and kinetic studies

To gain mechanistic insights into the new catalytic system, we carried out isotope effect[26] and kinetic studies.[27] The kinetic isotope effect (KIE = k_H/k_D) was examined using benzaldehyde **2a** with either HBpin or DBpin under the same conditions as in Table 1, with a carbonyl concentration of 0.05 M. A comparison of the initial rate plots (k_D) for HBpin and DBpin (Fig. S3) indicates a slower reaction with the deuterated borane, giving an observed KIE of 1.8(1) (1.5 by DFT calculations, *vide infra*). This KIE value is interpreted as a primary isotope effect, albeit modest, suggesting that the B–H bond is substantially weakened in the rate-determining step. Notably, this value is close to the KIE of 1.62 ± 0.13 reported by Hartwig *et al.* for B–H bond activation of catecholborane (HBcat) by a ruthenium complex $CpRu(PPh_3)_2(Me)$.[26a] In that system, the reaction is proposed to proceed *via* a four-centred transition state featuring a Ru–H–B(cat)–Me linkage.

Kinetic studies were also performed using benzaldehyde **2a** and HBpin under conditions similar to Table 1, with an aldehyde concentration of 0.05 M. Eyring plots were constructed based on the net initial rate constants, which were obtained by subtracting the contribution of the uncatalysed reaction background from the observed rates in the presence of **1** (see SI for details). Initial rate measurements were carried out at five temperatures ranging from 305 to 320 K. The Gibbs activation energy ($\Delta G^{\ddagger}$) for **2a** was determined to be 24.9(3) [kcal mol^{-1}], consistent with the reaction proceeding at room temperature (Table 3). The enthalpy of activation ($\Delta H^{\ddagger}$) was estimated to be 6.0(3) kcal mol^{-1}. The large negative entropy of activation [$\Delta S^{\ddagger}$ = −63(1) cal mol^{-1} K^{-1}] is indicative of an associative mechanism, suggesting the formation of a highly ordered transition state (*vide infra*).

Possible pathways

Based on these experimental results and the fundamental reactivity of germylyne complexes, where the substrate heteroatom

Table 3 Activation parameters for the catalytic hydroboration of benzaldehyde with HBpin mediated by **1**

	$\Delta G^{\ddagger}_{298.15K}$ [kcal mol^{-1}]	$\Delta H^{\ddagger}$ [kcal mol^{-1}]	$\Delta S^{\ddagger}$ [cal mol^{-1} K^{-1}]
Exp.[a]	24.9(3)	6.0(3)	−63(1)
Calc.[b]	25.0	6.7	−53.1

[a] From Eyring plot. [b] From DFT calculations at the PW6B95+D3BJ/Def2-TZVPP//PW6B95+D3BJ/Def2-SVP level. These activation energies are relative to **b** in Fig. 3.

consistently interacts with the tetrel centre, previously investigated by us,[28] we considered four possible pathways for this catalytic system (Fig. 2). The first pathway (1) involves CO dissociation from the 18-electron saturated complex **1**, generating a 16-electron unsaturated species **I**, which could undergo B–H oxidative addition of HBpin or allow the aldehyde to coordinate to the metal centre. However, our previous calculations suggest that species **II** is significantly higher in energy (ΔG = 51.1 kcal mol^{-1}) than complex **1** and is therefore thermally inaccessible.[23] The second pathway (2) involves B–H oxidative addition and aldehyde coordination through the formation of metallogermylene species **II**. Our DFT calculations, however, did not identify such a species as either an intermediate or a transition state. Instead, species **III**, featuring a six-membered ring, was identified as a transition state, suggesting that pathway (3) proceeds *via* a concerted H-migration mechanism, which will be discussed in detail in the following section. This mechanism is in line with our recent proposal for the hydrosilylation mechanism catalysed by complex **1**.[23] We also examined a direct B–H addition pathway (4) involving species **IV**, which resembles mechanisms occasionally proposed for other systems involving 1,2-addition of B–H to the C=O bond.[1,5,6] However, this route appears unlikely in this system because the calculated activation barrier is prohibitively high (39.3 kcal mol^{-1}; see Fig. S53 in the SI). Furthermore, the conventional mechanisms, such as those involving a metal hydride species[4] or a tetrylene hydride species[7] as the active catalyst, are unlikely in this case, as no *in situ* formation of either species was detected. Based on these results, we focused our detailed analysis on pathway (3).

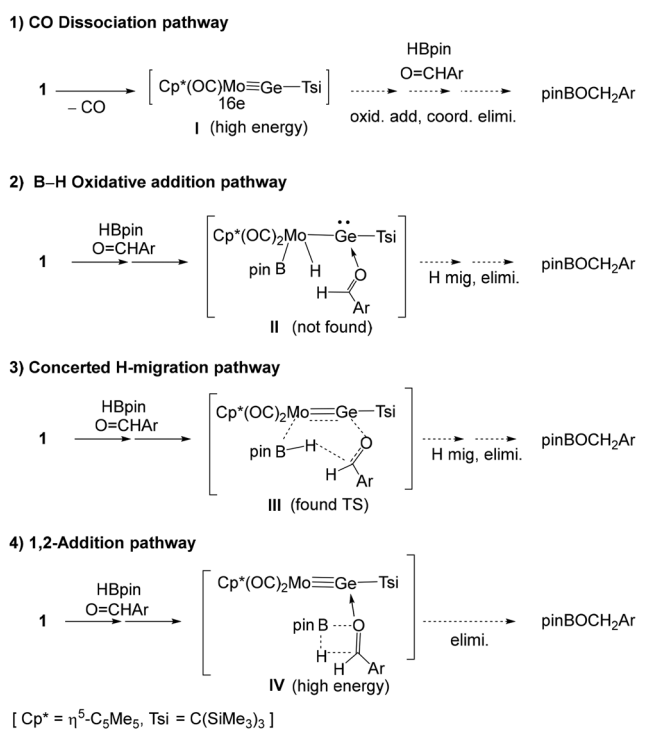

Fig. 2 Possible pathways for the catalytic mechanism *via* (1) CO dissociation pathway, (2) B–H oxidative addition pathway, (3), concerted H-migration and (4) 1,2-addition pathway.

Computational studies

DFT calculations were carried out for the hydroboration of benzaldehyde **2a** with HBpin as a representative case (Fig. 3, see also Table S3 in the SI). The optimised geometry of **1** was in good agreement with its crystallographically determined solid-state structure.[21] At the initial stage, we hypothesised that a Lewis acid–base adduct forms between HBpin and the aldehyde,[24] given that a measurable uncatalysed reaction occurs under these conditions.

Computational analysis

Identified an initial state (denoted as **a**) in which the borane–aldehyde adduct is formed and weakly interacts with complex **1**. Based on this model, the mechanistic study examined the Gibbs energy profile starting from state **a**, as shown in Fig. 3. The profile comprises two transition states (**TS-1** and **TS-2**, see also Fig. 4). The activation barrier associated with **TS-1** ($\Delta G^{\ddagger}_{298.15K}$ = 25.0 kcal mol^{-1}) is higher than that of **TS-2** (21.9 kcal mol^{-1}), making **TS-1** the rate-determining step. The calculated parameters for this step ($\Delta G^{\ddagger}_{298.15K}$ = 25.0 kcal mol^{-1}, $\Delta H^{\ddagger}$ = 6.7 kcal mol^{-1}, $\Delta S^{\ddagger}$ = −53.1 cal mol^{-1} K^{-1}) are in very good agreement with the experimental values ($\Delta G^{\ddagger}_{298.15K}$ = 24.9(3) kcal mol^{-1}, $\Delta H^{\ddagger}$ = 6.0(3) kcal mol^{-1}, $\Delta S^{\ddagger}$ = −63(1) cal mol^{-1} K^{-1}) (Table 1), supporting that the computed rate-determining step reliably reproduces the reaction energetics.

In the initial state **a**, the Mo–Ge distance (2.30 Å) of **a** remains essentially unchanged compared to that in free catalyst **1** (2.29 Å), while the borane and the aldehyde are significantly interacting (B⋯O distance, 2.90 Å). From state **a**, the borane–aldehyde adduct dissociates to give **b**, where the electrophilic Ge(I) centre interacts with the aldehyde oxygen.[29] This intermediate **b** represents shallow minima (ΔG = −8.3 kcal mol^{-1}) between the state **a** and the subsequent state **c**. In **b**, the Ge⋯O distance in **b** (2.46 Å) is longer than typical Ge ← O coordination bonds (1.8–2.1 Å),[30] indicating only weak coordination. Re-interaction of HBpin with the coordinated aldehyde in **b** gives **c**, where the borane hydride weakly interacts with the aldehyde carbon (H⋯C distance: 2.72 Å), accompanied by a slightly stronger Ge⋯O interaction (2.43 Å).

Next, a hydride migration occurs from the borane to the carbonyl carbon *via* transition state **TS-1** (Fig. 4), producing intermediate **d**. This phase can be considered the rate-determining step, as **TS-1** exhibits the highest activation barrier in the entire catalytic cycle. At **TS-1**, relative to intermediate **c**, the Mo–Ge bond elongates from 2.33 Å to 2.42 Å, which is close to the Mo=Ge bond length [2.4224(9) Å] of the synthetic precursor of **1**:[21] and falls within the typical range of Mo=Ge double bonds (2.38–2.56 Å).[31] The ∠(Mo–Ge–C(Tsi)) angle decreases only slightly from 155° to 151° by 4°. The resulting intermediate **d** exhibits a further weakened Mo=Ge bond (2.47 Å) while remaining within the typical double-bond range, and a bent Mo–Ge–C angle of 145°. These structural changes indicate that, in **TS-1**, both the borane and the aldehyde are cooperatively acti-

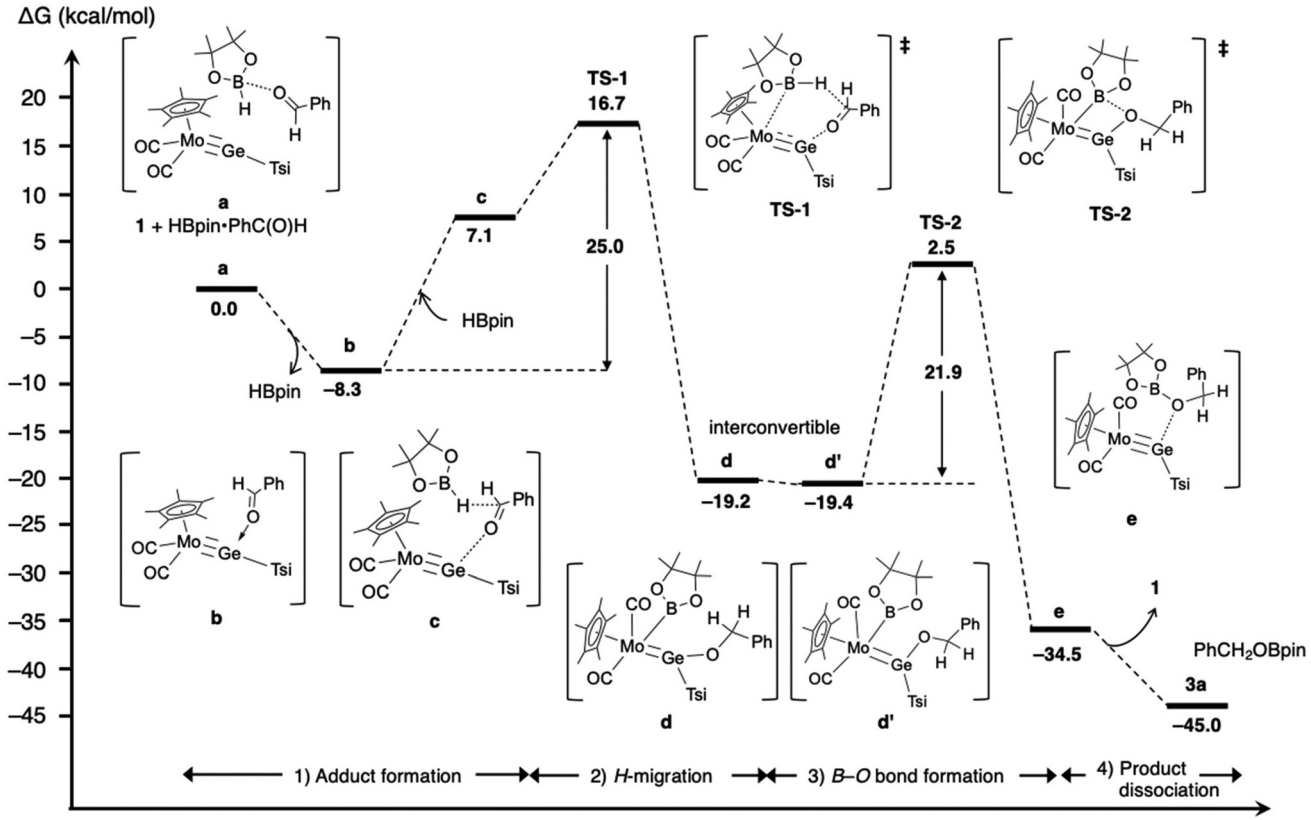

Fig. 3 Gibbs free energy profile for the hydroboration of PhC(O)H (**2a**) with HBpin catalysed by **1**.

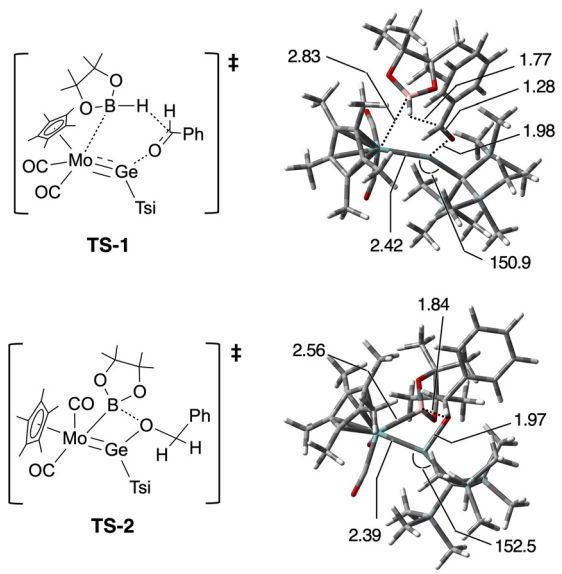

Fig. 4 Transition states **TS-1** and **TS-2** for the hydroboration of PhC(O)H with HBpin.

vated through concurrent Mo–B and Ge–O bond formation, while the Mo–Ge multiple bond is preserved yet flexibly modulated to facilitate this unique three-component interaction. Notably, the persistence of Mo–Ge multiple bonding in **TS-1** is further supported by molecular orbital analysis, revealing the presence of π-type orbitals (Fig. S52 in the SI). Intermediate **d** exists in a rapidly interconvertible conformation (**d′**), separated by only 0.2 kcal mol^{-1}, which is attributable to rotation around the Ge–O bond. Subsequent B–O bond formation proceeds through **TS-2**, yielding the product dissociation state **e**. In this step, B–O bond formation is accompanied by cleavage of the Mo–B bond and weakening of the Ge–O interaction, ultimately restoring the Mo≡Ge bond (2.39 Å).

It should be noted here that the electron density in **TS-1** is redistributed over the entire six-membered-ring framework, with negligible charge development on the aromatic ring (Ph), thereby minimizing the influence of *para*-substituents of aryl carbonyl substrates in this system, which may explain the experimental observation (*vide supra*). It should also be noted that the lower reactivity of aromatic aldehydes/ketones compared with aliphatic substrates has also been reported in other hydroboration systems.[13,17d] In our system, the rate-determining **TS-1** involves a six-membered-ring transition state, which could be affected by the steric bulk of the aryl ring. Hydride transfer to the carbonyl carbon in **TS-1** also appears less favourable for aryl substrates, due to π-conjugation between the aromatic ring with the carbonyl group. In contrast, smaller aliphatic aldehydes lack such π-stabilization and experience reduced steric congestion, which may contribute to their higher reactivity toward hydroboration.

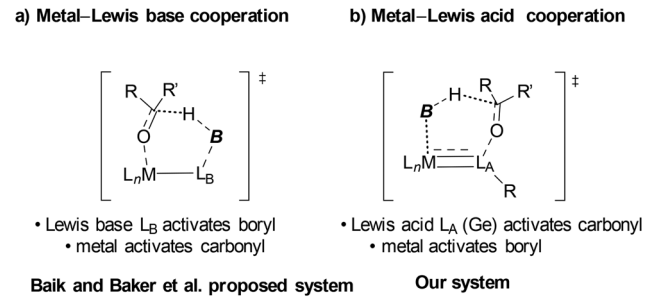

Fig. 5 Two types of transition states for carbonyl hydroboration: (a) metal-Lewis base cooperation and (b) metal-Lewis acid cooperation.

Overall, the catalytic mechanism presented in Fig. 3 confirms a novel mode of metal–ligand cooperativity in **1**: the transition metal activates the borane, while the Lewis acidic germylyne ligand activates the aldehyde. Importantly, this occurs without loss of the metal–ligand multiple-bond character. It should also be noted that Baik, Baker, and co-workers[10a] have recently proposed a relevant six-membered transition state for their Mn system bearing an SNS ligand. This activation is interpreted as metal-Lewis base cooperation (Fig. 5a), whereas our system operates through metal-Lewis acid cooperation (Fig. 5b).

Conclusions

We have demonstrated that molybdenum–germanium triple-bonded complex **1** efficiently catalyses the hydroboration of aldehydes at room temperature and of ketones at elevated temperatures. The novel mode of metal–ligand cooperativity across the metal–germanium triple bond is deduced by kinetic experiments and KIE studies, supported by DFT calculations, further corroborating the proposed mechanism. This study represents a significant step toward further realising the catalytic potential of tetrylyne complexes and related polarized multiple-bonded systems.

Author contributions

C. F. conducted experiments, performed theoretical studies and prepared the original manuscript. K. N. contributed to the theoretical studies and revision of the manuscript. S. I. and A. T. conducted kinetic experiments. Y. S. and S. M. performed theoretical studies. T. P. D. and S. I. synthesised the starting materials. H. H. conceived the idea of developing molybdenum germylyne complexes, directed the project, and finalised the manuscript. All authors contributed to the analysis and interpretation of the data and commented on the final draft of the manuscript.

Conflicts of interest

There are no conflicts to declare.

Data availability

The data supporting this article are included in the supplementary information (SI). Supplementary information: experimental procedures, characterisation data, kinetics, NMR spectra, DFT calculations, and atomic coordinates (*xyz*) for all optimised geometries. See DOI: https://doi.org/10.1039/d5dt02829a.

Acknowledgements

This work was supported by JSPS KAKENHI grants JP_22H02088, 23K23356 (HH), 19H04687 and 21K14638 (KN) from the Japan Society for the Promotion of Science (JSPS). We would like to thank Prof. Yasuhiro Ohki, Mr Kanata Tanaka and Dr Hitoshi Izu of the Institute for Scientific Research, Kyoto University, for providing the DBpin reagent used in KIE experiments. Computation was performed using the Research Centre for Computational Science, Okazaki, Japan (project: 22-IMS-C102, 23-IMS-C089, 24-IMS-C041, 24-IMS-C084, 25-IMS-C042 and 25-IMS-C086).

References

1 M. L. Shegavi and S. K. Bose, *Catal. Sci. Technol.*, 2019, **9**, 3307–3336.
2 K. Kuciński and G. Hreczycho, *Green Chem.*, 2020, **22**, 5210–5224.
3 S. J. Geier, C. M. Vogels, J. A. Melanson and S. A. Westcott, *Chem. Soc. Rev.*, 2022, **51**, 8877–8922.
4 C. C. Chong and R. Kinjo, *ACS Catal.*, 2015, **5**, 3238–3259.
5 S. Ramkumar, S. Reddappa, S. Mohan, K. Pramoda and S. K. Bose, *ChemCatChem*, 2025, **17**(14), e00206.
6 S. R. Tamang and M. Findlater, *Molecules*, 2019, **24**, 3194.
7 (*a*) S. K. Mandal and H. W. Roesky, *Acc. Chem. Res.*, 2012, **45**, 298–307; (*b*) M. M. D. Roy, A. A. Omaña, A. S. S. Wilson, M. S. Hill, S. Aldridge and E. Rivard, *Chem. Rev.*, 2021, **121**, 12784–12965.
8 (*a*) J. Schneider, C. P. Sindlinger, S. M. Freitag, H. Schubert and L. Wesemann, *Angew. Chem., Int. Ed.*, 2017, **56**, 333–337; (*b*) L. J. Bole, M. Uzelac, A. Hernán-Gómez, A. R. Kennedy, C. T. Óhara and E. Hevia, *Inorg. Chem.*, 2021, **60**, 13784–13796.
9 (*a*) Y. Wu, C. Shan, Y. Sun, P. Chen, J. Ying, J. Zhu, L. L. Liu and Y. Zhao, *Chem. Commun.*, 2016, **52**, 13799–13802; (*b*) V. A. Pollard, S. A. Orr, R. McLellan, A. R. Kennedy, E. Hevia and R. E. Mulvey, *Chem. Commun.*, 2018, **54**, 1233–1236.
10 (*a*) M. R. Elsby, M. Son, C. Oh, J. Martin, M.-H. Baik and R. T. Baker, *ACS Catal.*, 2021, **11**, 9043–9051; (*b*) S. Ataie, S. L. Dudra, E. R. Johnson and R. T. Baker, *ACS Catal.*, 2023, **13**, 10076–10084; (*c*) C. Ekren, A. Kaithal, S. Sen, T. Weyhermüller, M. Hölscher, C. Werlé and W. Leitner, *Nat. Chem.*, 2018, **9**, 4521.
11 (*a*) J. R. Khusnutdinova and D. Milstein, *Angew. Chem., Int. Ed.*, 2015, **54**, 12236–12273; (*b*) R. H. Morris, *Acc. Chem.*

Res., 2015, **48**, 1494–1502; (*c*) T. Higashi, S. Kusumoto and K. Nozak, *Chem. Rev.*, 2019, **119**, 10393–10402; (*d*) M. R. Elsby and R. T. Baker, *Chem. Soc. Rev.*, 2020, **49**, 8933–8987.

12 (*a*) P. P. Power, *Nature*, 2010, **463**, 171–177; (*b*) Y. Mizuhata, T. Sasamori and N. Tokitoh, *Chem. Rev.*, 2009, **109**, 3479–3511; (*c*) L. Wang, Y. Li, Z. Li and M. Kira, *Coord. Chem. Rev.*, 2022, **457**, 214413.

13 T. J. Hadlington, *Chem. Soc. Rev.*, 2024, **53**, 9738–9831.

14 (*a*) M. Okazaki, H. Tobita and H. Ogino, *Dalton Trans.*, 2003, 493–506; (*b*) R. Waterman, P. G. Hayes and T. D. Tilley, *Acc. Chem. Res.*, 2007, **40**, 712–721; (*c*) L. Álvarez-Rodríguez, J. A. Cabeza, P. García-Álvarez and D. Polo, *Coord. Chem. Rev.*, 2015, **300**, 1–28; (*d*) R. J. Somerville and J. Campos, *Eur. J. Inorg. Chem.*, 2021, 3488–3498; (*e*) M. Ghosh, N. Sen and S. Khan, *ACS Omega*, 2022, **7**, 6449–6454.

15 (*a*) T. J. Hadlington, M. Hermann, G. Frenking and C. Jones, *J. Am. Chem. Soc.*, 2014, **136**, 3028–3031; (*b*) Y. Wu, C. Shan, Y. Sun, P. Chen, J. Ying, J. Zhu, L. L. Liu and Y. Zhao, *Chem. Commun.*, 2016, **52**, 13799–13802; (*c*) H. J. Robertson, M. N. Fujiwara and L. Liberman-Martin, *Polyhedron*, 2024, **250**, 116837; (*d*) A. P. Khuntia, N. Sarkar, A. G. Patro, R. K. Sahoo and S. Nembenna, *Eur. J. Inorg. Chem.*, 2022, **20**, e202200209; (*e*) M. M. D. Roy, S. Fujimori, M. J. Ferguson, R. McDonald, N. Tokitoh and E. Rivard, *Chem. – Eur. J.*, 2018, **24**, 14392–14399; (*f*) S. Sinhababu, D. Singh, M. K. Sharma, R. K. Siwatch, P. Mahawar and S. Nagendran, *Dalton Trans.*, 2019, **48**, 4094–4100; (*g*) D. Sarkar, S. Dutta, C. Weetman, E. Schubert, D. Koley and S. Inoue, *Chem. – Eur. J.*, 2021, **27**, 13072–13078; (*h*) K. V. Arsenyeva, K. I. Pashanova, O. Y. Trofimova, I. V. Ershova, M. G. Chegerev, A. A. Starikova, A. V. Cherkasov, M. A. Syroeshkin, A. Ya. Kozmenkova and A. V. Piskunov, *New J. Chem.*, 2021, **45**, 11758–11767.

16 (*a*) K. Nakaya, S. Takahashi, A. Ishii, K. Boonpalit, P. Surawatanawong and N. Nakata, *Dalton Trans.*, 2021, **50**, 14810–14819; (*b*) R. Dasgupta, S. Das, S. Hiwase, S. K. Pati and S. Khan, *Organometallics*, 2019, **38**, 1429–1435; (*c*) Y. Liu, X. Liu, Y. Liu, W. Li, Y. Ding, M. Zhong, X. Ma and Z. Yang, *Inorg. Chim. Acta*, 2018, **471**, 244–248; (*d*) M. Zhong, Y. Ding, D. Jin, X. Ma, Y. Liu, B. Yan, Y. Yang, J. Peng and Z. Yang, *Inorg. Chim. Acta*, 2019, **486**, 669–674; (*e*) M. K. Sharma, M. Ansari, P. Mahawar, G. Rajaraman and S. Nagendran, *Dalton Trans.*, 2019, **48**, 664–672; (*f*) V. Nesterov, R. Baierl, F. Hanusch, A. E. Ferao and S. Inoue, *J. Am. Chem. Soc.*, 2019, **141**, 14576–14580; (*g*) Y. Kobayashi, K. Nakaya, S. Takahashi, R. Watanabe and N. Nakata, *Chem. – Eur. J.*, 2025, **31**, e20250139; (*h*) S. Pahar, V. Sharma, S. Tothadi and S. S. Sen, *Dalton Trans.*, 2021, **50**, 16678–16684.

17 (*a*) J. Lee, J. Fan, A.-P. Koh, W.-J. J. Cheang, M.-C. Yang, M.-D. Su and C.-W. So, *Eur. J. Inorg. Chem.*, 2022, **19**, e202200129; (*b*) X. Qi, T. Zheng, J. Zhou, Y. Dong, X. Zuo, X. Li, H. Sun, O. Fuhr and D. Fenske, *Organometallics*, 2019, **38**, 268–277; (*c*) S. Khoo, J. Cao, F. Ng and C.-W. So, *Inorg. Chem.*, 2018, **57**, 12452–12455; (*d*) L. Kapp, C. Wölper, H. Siera, G. Haberhauer and S. Schulz, *Chem. Sci.*, 2024, **15**, 4161–4170; (*e*) B.-X. Leong, J. Lee, Y. Li, M.-C. Yang, C.-K. Siu, M.-D. Su and C.-W. So, *J. Am. Chem. Soc.*, 2019, **141**, 17629–17636; (*f*) G. Zhang, S. Li, H. Zeng, S. Zheng and M. C. Neary, *RSC Adv.*, 2022, **12**, 19086–19090; (*g*) K. Nakaya, S. Takahashi, A. Ishii and N. Nakata, *Inorg. Chem.*, 2022, **61**, 15510–15519.

18 (*a*) P. B. Glaser and T. D. Tilley, *J. Am. Chem. Soc.*, 2003, **125**, 13640–13641; (*b*) E. Calimano and T. D. Tilley, *J. Am. Chem. Soc.*, 2009, **131**, 11161–11173; (*c*) E. Calimano and T. D. Tilley, *Organometallics*, 2010, **29**, 1680–1692.

19 T. Muraoka, Y. Shimizu, H. Kobayashi, K. Ueno and H. Ogino, *Organometallics*, 2010, **29**, 5423–5426.

20 (*a*) H. Hashimoto and H. Tobita, *Coord. Chem. Rev.*, 2018, **355**, 362–379; (*b*) H. Hashimoto and K. Nagata, *Chem. Lett.*, 2021, **50**, 778–787; (*c*) L. R. Maurer, J. Rump and A. C. Filippou, *Inorganics*, 2023, **11**, 129; (*d*) N. Takagi, K. Yamazaki and S. Nagase, *Bull. Korean Chem. Soc.*, 2003, **24**, 832–836; (*e*) K. K. Pandey, P. Patidar and P. P. Power, *Inorg. Chem.*, 2011, **50**, 7080–7089.

21 T. P. Dhungana, H. Hashimoto, M. Ray and H. Tobita, *Organometallics*, 2020, **39**, 4350–4361.

22 T. P. Dhungana, H. Hashimoto, K. Nagata and H. Tobita, Catalytic Hydrosilylation of Carbonyl Compounds by a Germylyne Complex with a Mo≡Ge Triple Bond, *ChemRxiv*, 2025, preprint, DOI: 10.26434/chemrxiv-2025-1hc87, https://chemrxiv.org/engage/chemrxiv/article-details/6901bf08a482cba122a3eab5.

23 T. P. Dhungana, N. Takagi, B. Zhu, K. Nagata, S. Sakaki, H. Tobita and H. Hashimoto, Mechanistic Insights into Catalytic Hydrosilylation of Carbonyl Compounds *versus* [2 + 2] Cycloaddition Pathway Mediated by Germylyne Complexes, *ChemRxiv*, 2025, preprint, DOI: 10.26434/chemrxiv-2025-8tqj5, https://chemrxiv.org/engage/chemrxiv/article-details/690c0d51113cc7cfff6c10ff.

24 H. Stachowiak, J. Kaźmierczak, K. Kuciński and G. Hreczycho, *Green Chem.*, 2018, **20**, 1738–1742.

25 The TOF of 2.1 h^{-1} was estimated by us using data reported in the literature (ref. 9*a*).

26 (*a*) J. F. Hartwig, S. Bhandari and P. R. Rablen, *J. Am. Chem. Soc.*, 1994, **116**, 1839–1844; (*b*) X. Gao, X.-Y. Yu and C.-R. Chang, *Phys. Chem. Chem. Phys.*, 2022, **24**, 15182–15194; (*c*) E. M. Simmons and J. F. Hartwig, *Angew. Chem., Int. Ed.*, 2012, **51**, 3066–3072; (*d*) M. Gómez-Gallego and M. A. Sierra, *Chem. Rev.*, 2011, **111**, 4857–4963.

27 A. S. Chang, K. E. Kawamura, H. S. Henness, V. M. Salpino, J. C. Greene, L. N. Zakharov and A. K. Cook, *ACS Catal.*, 2022, **12**, 11002–11014.

28 (*a*) H. Hashimoto, T. Fukuda, H. Tobita, M. Ray and S. Sakaki, *Angew. Chem., Int. Ed.*, 2012, **51**, 2930–2933; (*b*) T. Fukuda, H. Hashimoto and H. Tobita, *Chem. Commun.*, 2013, **49**, 4232–4234; (*c*) T. Fukuda, H. Hashimoto and H. Tobita, *J. Am. Chem. Soc.*, 2014, **136**, 80–83; (*d*) T. Yoshimoto, H. Hashimoto, N. Hayakawa,

T. Matsuo and H. Tobita, *Organometallics*, 2016, **35**, 3444–3447; (*e*) T. Yoshimoto, H. Hashimoto, N. Takagi, S. Sakaki, N. Hayakawa, T. Matsuo and H. Tobita, *Chem. – Eur. J.*, 2019, **25**, 3795–3798; (*f*) K. Nagata, H. Omura and H. Hashimoto, *Chem. – Asian J.*, 2023, **18**, e202300801.

29 The NPA charges (Mo: −1.44; Ge: +1.35) indicate that the Ge atom in complex **1** bears a significant positive charge, consistent with its role as the primary Lewis acidic site in the cooperative activation of HBpin and carbonyl substrates (Table S4).

30 M. Iglesias, F. J. Fernández-Alvarez and L. A. Oro, *Coord. Chem. Rev.*, 2019, **386**, 240–266.

31 Based on a survey of the Cambridge Structural Database and CSD version 5.46 (November 2024).